Journal of
Materials Chemistry C

Materials for optical, magnetic and electronic devices

Accepted Manuscript

This article can be cited before page numbers have been issued, to do this please use: M. Gon, C. Ma and K. Tanaka, *J. Mater. Chem. C*, 2026, DOI: 10.1039/D6TC00672H.

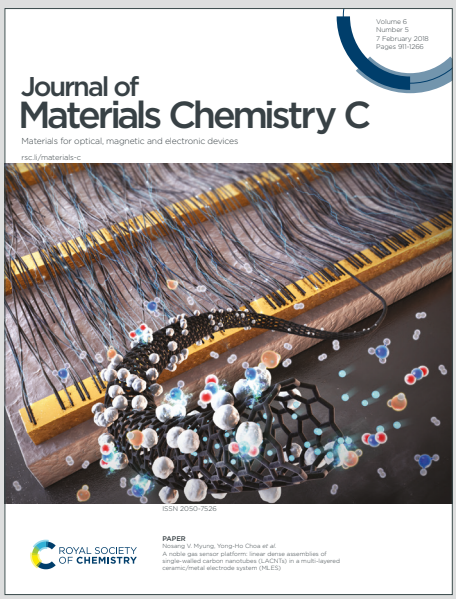

ROYAL SOCIETY OF CHEMISTRY

rsc.li/materials-c

View Article Online
DOI: 10.1039/D6TC00672H

Development of Visible-to-NIR Light Absorbing and Emitting Polymers Incorporating Hypervalent Germafluorene-Fused π-Conjugated Systems

Masayuki Gon[1,2], Chentian Ma[1], and Kazuo Tanaka[1,2]*

[1]*Department of Polymer Chemistry, Graduate School of Engineering, Kyoto University Katsura, Nishikyo-ku, Kyoto 615-8510, Japan*

[2] *Department of Technology and Ecology, Graduate School of Global Environmental Studies, Kyoto University, Katsura, Nishikyo-ku, Kyoto 615-8510, Japan*

E-mail: tanaka@poly.synchem.kyoto-u.ac.jp

Keywords: germanium; hypervalent compound; π-conjugated polymer; spiroconjugation; near-infrared light

View Article Online
DOI: 10.1039/D6TC00672H

Abstract

Novel molecular designs for creating near-infrared (NIR) light absorbing and emitting materials are required to meet growing demands for NIR light-based technologies. Herein, we demonstrate that the five-coordinate hypervalent germanium (Ge) compounds composed of germafluorene-fused azomethine and azo scaffolds with efficient light absorption and emission in the visible-to-NIR region (λ_{abs} = 505–902 nm, λ_{PL} = 667–1014 nm, Φ_{PL} up to 18.1%). These excellent optical properties are attributed to the hypervalent Ge-centered spiroconjugation and their planar π-conjugated systems. Experimental and theoretical data indicate that the spiroconjugation plays a significant role in the elevation of the HOMO (highest occupied molecular orbital) energy level. Moreover, the introduction of bulky substituents at the germafluorene moiety contributes to enhancing planarity of the π-conjugated systems, which further narrows their energy gaps. Since the bulky substituents not only improved processability but also suppressed intermolecular interactions, efficient NIR emission was also observed in polymer films. These results suggest that the integration of hypervalent states with π-conjugated systems can be one of effective strategies for tuning electronic properties of NIR light absorbing and emitting materials.

View Article Online
DOI: 10.1039/D6TC00672H

Introduction

Near-infrared (NIR) light has attracted considerable attention because of its unique features, such as invisibility to the human eye, high biotissue permeability, and smaller light scattering compared with visible light.[1,2] Therefore, the development of NIR light absorbing and emitting materials has been actively pursued, and a variety of chemical scaffolds have been proposed, such as cyanine, squaraine, rhodamine, boron dipyrromethene (BODIPY), and donor–acceptor (D–A) dyes (Figure 1a).[3,4] However, wide π-conjugated systems are generally needed to achieve the narrow energy gaps for NIR light absorption and emission. Consequently, it is often challenging to tune the optical properties of such π-conjugated systems through chemical modification and polymerization due to their low solubility and intrinsic structural constraints of their π-conjugated frameworks. Moreover, solid-state luminescence is often diminished by concentration quenching originating from non-specific intermolecular interactions in the condensed state.[5] From above reasons, the development of compact and versatile molecular structures to afford NIR light absorption and emission remains highly desirable.

The introduction of heteroatoms into chemical backbones is an effective strategy for tuning optical properties without altering the molecular skeletons.[6–19] We have recently proposed that the replacement of the skeletal carbon atom with a nitrogen atom at the "isolated frontier molecular orbital (FMO)" position, where only one of FMOs is distributed in the π-conjugated system, provides a facile protocol for selectively modulating an energy level of one of FMOs.[20,21] Based on this concept, π-conjugated systems incorporating azomethine (Ar-CH=N-Ar) and azo (Ar-N=N-Ar) scaffolds represent promising candidates for lowering the lowest unoccupied molecular orbital (LUMO) energy levels from those including vinylene (Ar-CH=CH-Ar) scaffolds (Figure

View Article Online
DOI: 10.1039/D6TC00672H

1b).[22–24] Since the vinylene unit is one of the famous π-conjugated linkers for showing excellent optical properties,[25,26] the utilization of azomethine and azo scaffolds is expected to provide both structural versatility and superior optical properties in the field of NIR chemistry.

It is known that π-conjugated systems containing azomethine and azo moieties tend to be non-emissive due to fast internal conversion of the excited energy *via* non-radiative deactivation pathways often accompanied by *cis–trans* photoisomerization.[27–32] Recently, it has been reported that boron coordination at these units markedly alters their electronic properties, thereby inducing bright emission.[33,34] Our research group has also found that boron-fused azomethine and azo (BAm and BAz) scaffolds exhibit aggregation-induced emission (AIE) and crystallization-induced emission (CIE) (Figure 1c).[35,36] In AIE and CIE-active materials, the emission is quenched in solution, while emission enhancement occurs in aggregate and crystalline formation, respectively.[37–39] BAm and BAz scaffolds can also be used as electron-accepting comonomers for highly emissive D–A type π-conjugated polymers in the yellow-to-NIR region.[40,41] This is because boron–nitrogen (B–N) coordination additionally lowers the LUMO energy levels of the azomethine and azo moieties owing to the Lewis acidity of the boron center.

More recently, we have revealed that hypervalent heavy element-fused azomethine and azo compounds such as gallium (Ga)[42], tin (Sn)[43–45], germanium (Ge)[46,47], silicon (Si)[48,49], bismuth (Bi)[50], and antimony (Sb)[51] show absorption and emission bands in the longer wavelength region than their boron (B) analogues (Figure 1c). This unique bathochromic shift was attributed to a polarized hypervalent bond consisting of a three-center four-electron (3c-4e) bond around the hypervalent heavy element center.[52–61] Among these elements, hypervalent Ge compounds possess narrower energy gaps owing

View Article Online
DOI: 10.1039/D6TC00672H

to their less distorted trigonal bipyramidal geometry, in which the electronic perturbation from the 3c-4e bond to the π-conjugated system operates effectively.[46,60–63] Consequently, we previously observed efficient NIR emission reaching 800 nm from hypervalent Ge-fused compounds incorporating azobenzene-based π-conjugated systems.[46,47] However, it has been still challenging to realize structural diversity because hypervalent Ge compounds often decompose under prolonged and harsh reaction conditions, such as those used in polymerization.[46] Although there is such a synthetic difficulty, we considered the development of novel hypervalent Ge compounds has the potential to create materials exhibiting further bathochromically shifted NIR absorption and emission.

Herein, to achieve a further narrowing of the energy gaps in hypervalent Ge compounds while maintaining sufficient chemical stability, we introduced germafluorene scaffolds exhibiting hypervalent Ge-centered spiroconjugation (Figure 1e). Spiroconjugation refers to the interaction between two orthogonally oriented π-conjugated systems that share a single spiro atom (Figure 1d).[64–66] Unlike typical π-conjugation where double bonds and single bonds alternate, delocalization of π-electrons occurs even in a stereochemically twisted arrangement. In addition, by introducing a heavy element as a spiro center, it is known to further modulate the energy levels of the π-conjugated systems.[67,68] Although hypervalent elements can be spiro centers with higher coordination states, their electronic effects on π-conjugated systems have been hardly evaluated.[69–75] In our system, it was revealed that the hypervalent Ge spiro center within the germafluorene scaffold plays a significant role in narrowing the energy gap of the hypervalent Ge-fused azomethine and azo (GAm and GAz) compounds. This spiroconjugation is mainly attributed to an increase in HOMO energy levels of the azomethine- and azo-based π-conjugated system. In addition, we found that bulky

View Article Online
DOI: 10.1039/D6TC00672H

substituents on the germafluorene unit can enhance planarity of π-conjugated system, leading to a further narrowing of the energy gaps between FMOs. Moreover, the bulky substituents also improve chemical stability of the hypervalent Ge compounds. Thanks to these advantageous properties, we can synthesize various types of π-conjugated copolymers and show tuning of the optical properties in the visible-to-NIR region. We also demonstrate that a polymer nanoparticle (NP) exhibited the second NIR (NIR-II) emission (λ_{PL} = 1014 nm) in deionized H_2O owing to the high chemical stability and good solubility of the hypervalent germafluorene-fused π-conjugated materials. NIR-II emission (λ > 1000 nm) has been recognized as a powerful tool for deep-tissue biological imaging.[3,4] From these findings, we can say that the hypervalent Ge-fused compounds can be versatile units for constructing NIR light absorbing and emitting materials.

View Article Online
DOI: 10.1039/D6TC00672H

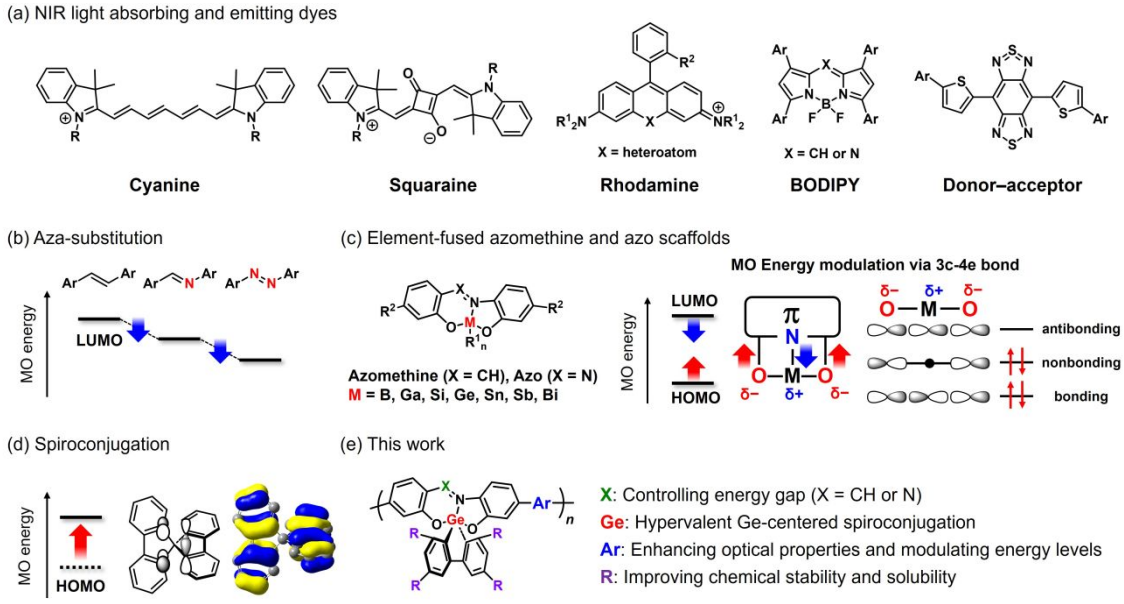

Figure 1. Research background and concept of this work. (a) General chemical structures of NIR light absorbing and emitting dyes. (b) Molecular orbital (MO) energy modulation via aza-substitution in a vinylene-based π-conjugated system. (c) General chemical structures of element-fused azomethine and azo scaffolds and MO energy modulation via 3c-4e bond in hypervalent element-fused π-conjugated systems. (d) MO energy modulation via spiroconjugation in spirobifluorene. (e) A molecular design strategy for narrowing the energy gap of a π-conjugated system based on a hypervalent Ge compound to develop visible-to-NIR light absorbing and emitting materials.

View Article Online
DOI: 10.1039/D6TC00672H

Results and Discussion

Synthesis

Scheme 1 shows the syntheses of hypervalent germafluorene-fused azomethine and azo monomers (**GAmFl-Br** and **GAzFl-Br**). By reacting each brominated tridentate ligand **AmOH-Br** and **AzOH-Br** with 2,4,6,8-tetra-*tert*-butyl-5,5-dichloro-5*H*-dibenzo[b,d]germole (**FlGeCl2**)[67] in the presence of triethylamine (Et_3N), the corresponding compounds **GAmFl-Br** and **GAzFl-Br** were obtained. The *tert*-butyl groups on the germafluorene moiety were introduced not only for improving the chemical stability of the hypervalent compounds by sterically shielding the reactive Ge center from nucleophilic attack[46,63] but also for enhancing solubility and planarity of the resulting π-conjugated systems. As model compounds, Ge-fused azomethine and azo compounds with phenyl substituents on the Ge atom (**GAmPh-Br** and **GAzPh-Br**) were also prepared (Scheme 1). **GAzPh-Br** was synthesized according to the method described in our previous literature.[47]

Next, we synthesized π-conjugated alternating copolymers containing the germafluorene-fused azomethine and azo units in the main chain (Scheme 2). The Migita–Kosugi–Stille cross-coupling[76,77] polymerizations with **GAmFl-Br** or **GAzFl-Br** and fluorene (**FL**) or bithiophene (**BT**), or cyclopentadithiophene (**CDT**) comonomers were carried out under a catalytic condition using $Pd_2(dba)_3$ (dba = dibenzylideneacetone) and 2-dicyclohexylphosphino-2′,4′,6′-triisopropylbiphenyl (XPhos) to provide six types of copolymers, **P-GAmFl-Ar** and **P-GAzFl-Ar** (**Ar** = **FL**, **BT**, **CDT**). The relative molecular weights of the products were determined by gel permeation chromatography (GPC) with polystyrene standards by using chloroform ($CHCl_3$) as an eluent (Figure S1 and Table 1). The resulting polymeric compounds showed good solubility in common

View Article Online
DOI: 10.1039/D6TC00672H

organic solvents such as toluene, $CHCl_3$, dichloromethane and tetrahydrofuran (THF). In addition, all synthesized compounds were characterized by ^1H and $^{13}C\{^1H\}$ NMR spectroscopy, high-resolution mass spectrometry (HRMS) (see the Electronic Supplementary Information, ESI) and had enough stability to use them under ambient conditions. From the characterization data, we concluded that the samples had the target structures and enough purity for further analyses.

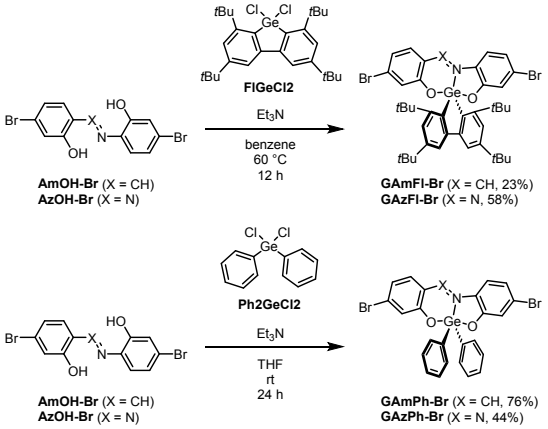

Scheme 1. Syntheses of the hypervalent Ge-fused azomethine and azo compounds.

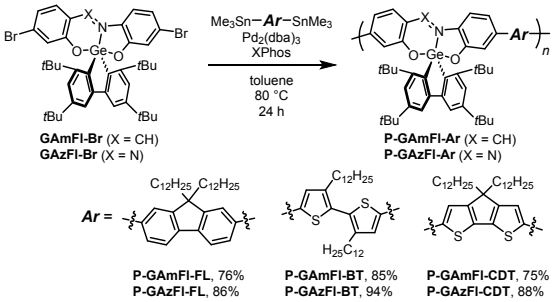

Scheme 2. Syntheses of the π-conjugated alternating copolymers containing hypervalent Ge moieties in the main chain. The regiorandom polymers are obtained and only a certain structure is shown here.

View Article Online
DOI: 10.1039/D6TC00672H

Table 1. Results of polymerizations

	M_n [a]	M_w [a]	M_w/M_n	DP_n [b]
P-GAmFl-FL	7,400	12,200	1.65	6.4
P-GAmFl-BT	13,000	37,500	2.89	11.2
P-GAmFl-CDT	17,400	43,200	2.49	14.9
P-GAzFl-FL	5,800	8,600	1.49	5.0
P-GAzFl-BT	13,700	30,500	2.22	11.8
P-GAzFl-CDT	9,600	19,200	2.00	8.2

[a] Determined by a gel permeation chromatography (GPC) with polystyrene standards in $CHCl_3$ as an eluent, M_n: number-average molecular weight, M_w: weight-average molecular weight. [b] Number-average degree of polymerization.

Crystal structure

We successfully obtained the single crystals of **GAmPh-Br** and **GAmFl-Br**, and their structures were investigated by the single crystal X-ray diffraction (SC-XRD) analysis (Figures 2, S2, and S3 and Tables S1–S3). The results clearly indicate not only the formation of five-coordinate hypervalent Ge compounds with distorted trigonal bipyramidal geometries[46,47,62,63] but also the presence of the germafluorene structure. **GAmFl-Br** exhibits a more planar azomethine-based π-conjugated system than **GAmPh-Br**, although their overall structural features are largely similar. The O(1)−Ge(1)−O(2) angles of **GAmPh-Br** and **GAmFl-Br** were 167.7° and 167.2°, respectively. This means there is little difference in the linearity of the 3c-4e bonds.[46] The N(1)−C(13) bond lengths of **GAmPh-Br** and **GAmFl-Br** were 1.298 Å and 1.295 Å, respectively. This indicates that these bonds can be assigned as C=N bonds. The Ge(1)−N(1) bond lengths of **GAmPh-Br** and **GAmFl-Br** were 2.004 Å and 2.008 Å, respectively. These data suggest that the introduction of the germafluorene unit hardly affected either the bond lengths or

View Article Online
DOI: 10.1039/D6TC00672H

the Ge–N interaction. On the other hand, the absolute values of dihedral angles of C(1)–N(1)–C(13)–C(7) and C(2)−O(1)−O(2)−C(8) were 178.3° and 33.22° for **GAmPh-Br**, 179.6° and 11.96° for **GAmFl-Br**, respectively. These results suggest that bulky substituents on the germafluorene moiety suppress distortion of the π-conjugated system by sterically protecting both sides of the π-surface. Thus, effective π-conjugation can be maintained without altering other structural parameters. Considering orthogonal arrangement of the germafluorene moiety and the azomethine-based π-conjugated system in **GAmFl-Br**, the occurrence of spiroconjugation is anticipated.

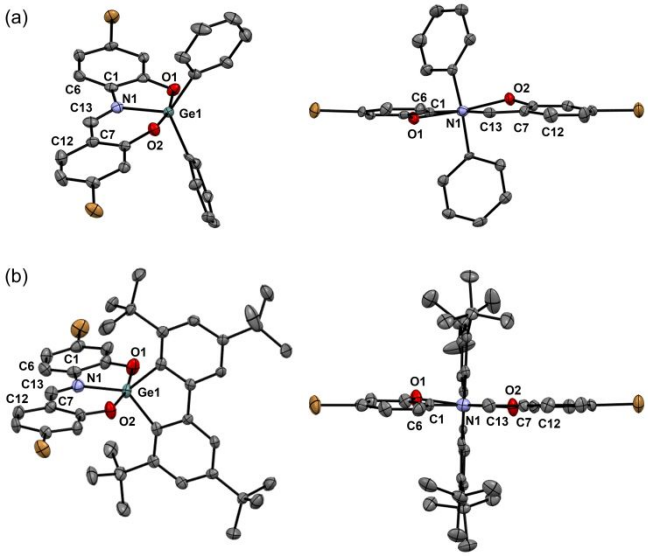

Figure 2. ORTEP drawings of (a) **GAmPh-Br** and (b) **GAmFl-Br** (50% probability for thermal ellipsoids). Hydrogen atoms and minor conformations are omitted for clarity. All crystallographic data are shown in the ESI.

View Article Online
DOI: 10.1039/D6TC00672H

Optical Properties

To investigate optical properties of the hypervalent Ge compounds, we performed UV–vis–NIR absorption and photoluminescence (PL) measurements with the diluted solutions (1.0×10^{-5} M in $CHCl_3$) and films. The results are summarized in Figure 3 and Table 2. Accordingly, the hypervalent Ge compounds exhibited broad absorption and emission bands in the wide wavelength region from the visible-to-NIR region depending on their chemical structures. In particular, the introduction of the germafluorene skeleton induced the distinct bathochromic shifts in the absorption and emission bands. These data indicate that the electronic perturbation of the azomethine- and azo-based π-conjugated systems through spiroconjugation and the resulting planar π-conjugated system contribute to narrowing the energy gaps. Additionally, the further bathochromic shifts in absorption and emission bands were observed by polymerization accompanied by improving emission efficiency. To comprehend emission mechanisms, a radiative rate constants (k_r) and a non-radiative rate constant (k_{nr}) were estimated from PL lifetime measurements (Figures S4 and S5). In the monomers, the k_r values were on the order of 10^7 s^{-1}. In contrast, in the polymers, the k_r values were increased to the order of 10^8 s^{-1}, which is the main factor responsible for the improved emission efficiency. Efficient emission was maintained in the NIR region beyond 700 nm despite the gradual increase in the k_{nr} values. Interestingly, in the polymer films, bathochromic shifts in the absorption and emission wavelengths were hardly observed compared to those in solution. This suggests that polymer aggregation is suppressed owing to steric protection provided by the bulky substituents on the germafluorene moiety. This effect is also favorable for improving solubility and processability, which are advantageous for polymer materials.

View Article Online
DOI: 10.1039/D6TC00672H

Table 2. Spectroscopic data of hypervalent Ge compounds

	λ_{abs} [b] /nm	λ_{PL} [b] /nm	Φ_{PL} [b,c,d] /%	τ_{av} [b,e]/ns	k_r [f] /10^8 s^{-1}	k_{nr} [f] /10^8 s^{-1}
GAmPh-Br	473	634	9.6	1.2	0.78	7.3
GAmFl-Br	505	663	6.7	1.0	0.66	9.2
P-GAmFl-FL	553	684	13.3	0.81	1.7	11
	(557) [g]	(691) [g]	(4.6) [g]	(0.44) [g]	(1.0) [g]	(22) [g]
P-GAmFl-BT	575	667	18.0	0.80	2.2	10
	(577) [g]	(690) [g]	(5.6) [g]	(0.43) [g]	(1.3) [g]	(22) [g]
P-GAmFl-CDT	700	744	8.5	0.26	3.3	35
	(687) [g]	(743) [g]	(2.0) [g]	(<0.1) [g]	(−[h]) [g]	(−[h]) [g]
GAzPh-Br [a]	570	715	2.6	0.37	0.70	26
GAzFl-Br	606	747	1.2	0.28	0.43	35
P-GAzFl-FL	678	776	3.2	0.27	1.2	36
	(682) [g]	(797) [g]	(2.0) [g]	(0.19) [g]	(1.1) [g]	(52) [g]
P-GAzFl-BT	723	819	4.4	0.25	1.8	38
	(731) [g]	(845) [g]	(2.6) [g]	(<0.1) [g]	(−[h]) [g]	(−[h]) [g]
P-GAzFl-CDT	902	982	0.6	−[h]	−[h]	−[h]
	(898) [g]	(974) [g]	(0.2) [g]	(−[h]) [g]	(−[h]) [g]	(−[h]) [g]

[a] From ref. 47. [b] In $CHCl_3$ (1.0×10^{-5} M for monomers and 1.0×10^{-5} M per repeating unit for polymers). [c] Excited at λ_{abs}. [d] Determined as an absolute value in the integrating sphere. [e] PL lifetimes monitored at λ_{PL}, excited at 504 nm with a diode laser. [f] $k_r = \Phi_{PL}/\tau_{av}$, $k_{nr} = (1 - \Phi_{PL})/\tau_{av}$, τ_{av}; average PL lifetime. [g] In film. [h] Not measured or not calculated.

View Article Online
DOI: 10.1039/D6TC00672H

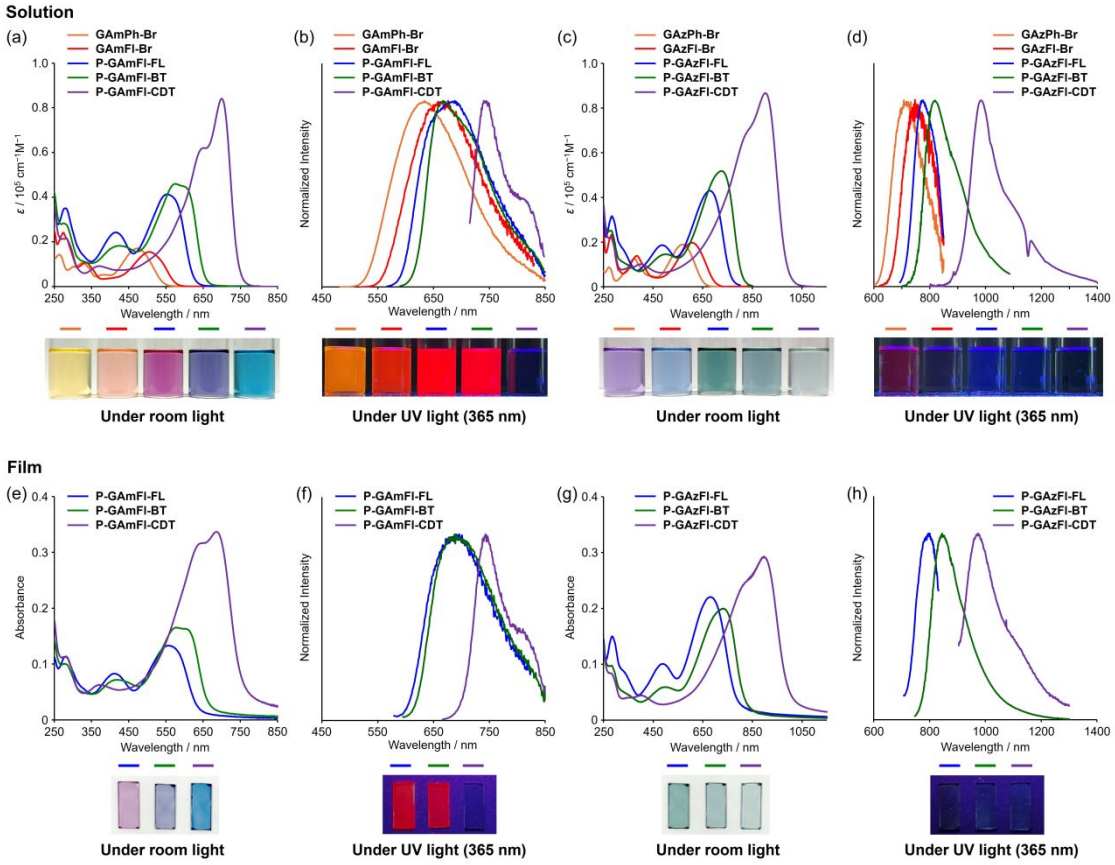

Figure 3. (a,c,e,g) UV–vis–NIR absorption and (b,d,f,h) PL spectra of hypervalent Ge compounds in $CHCl_3$ (1.0×10^{-5} M for monomers and 1.0×10^{-5} M per repeating unit for polymers) and in film, excited at wavelengths of absorption maxima. Some signal noise was observed due to the weak emission intensity of the samples and the low sensitivity of the photomultiplier tube (PMT) sensor in the long-wavelength region. Because of detector switching, PL spectra with maxima below 810 nm do not include the longer-wavelength region (≥850 nm) which cannot be detected using the PMT. Photographs of the hypervalent Ge compounds under room light and UV light (365 nm) are also shown in each figure.

View Article Online
DOI: 10.1039/D6TC00672H

Cyclic Voltammetry

Cyclic voltammetry (CV) were executed to experimentally investigate the origin of the energy-gap differences in the hypervalent Ge compounds. We estimated the HOMO and LUMO energy levels from onset potentials of oxidation and reduction curves in voltammogram, respectively (Figures 4 and S6, Table S4).[78,79] Accordingly, only minor changes in the HOMO and LUMO energy levels were observed upon introduction of the germafluorene structure (**GAmFl-Br** and **GAmFl-Br**) compared to the diphenylgermane compounds (**GAmPh-Br** and **GAmPh-Br**) (Figure 4). This result is inconsistent with that obtained from the optical measurements, suggesting that the effect of spiroconjugation may be difficult to detect by CV. In this point, further investigation was conducted in the next section through theoretical calculations. The LUMO energy levels were significantly lowered by employing the azo-based π-conjugated system compared to the azomethine-based one, which is the main factor responsible for narrowing the energy gap of the hypervalent Ge compounds. This effect originates from replacement of the methine carbon with a more electronegative nitrogen atom, and such selective control of molecular orbital (MO) energy levels has been reported by our group as the concept of the aza-substitution.[20,21] In the polymers, the azomethine- and azo-based hypervalent Ge compounds were found to exhibit similar trends in their HOMO energy levels depending on the electron-donating abilities of the comonomers **FL**, **BT**, and **CDT**. These results suggest that the D–A systems are formed within the polymers, in which the hypervalent Ge moiety acts as the acceptor, and the **FL**, **BT**, and **CDT** units act as the donors.

We compared the electronic energy gaps obtained from CV data ($E_{g,CV}$) with the optical energy ones derived from the onset wavelengths in the UV–vis–NIR absorption spectra ($E_{g,opt}$). As a result, good agreement between $E_{g,CV}$ and $E_{g,opt}$ was observed from

View Article Online
DOI: 10.1039/D6TC00672H

GAmPh-Br, **GAzPh-Br**, **P-GAmCDT**, and **P-GAzCDT**, whereas slight discrepancies were obtained from the other compounds (Table S4). Furthermore, these deviations were much clearer in the compounds with spiroconjugation and in weak D–A interaction. This tendency is consistent with the previous observations that the effect of spiroconjugation may be difficult to detect by CV. In addition, when the roles of the donor and acceptor units are not clearly separated, discrepancies between redox and optical properties are likely to arise.

View Article Online
DOI: 10.1039/D6TC00672H

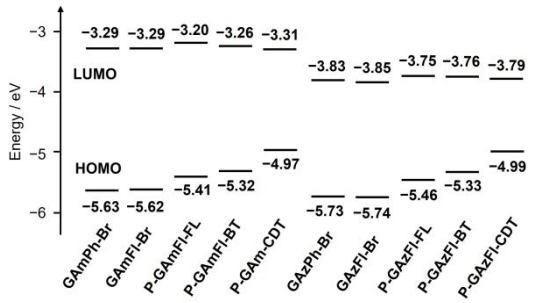

Figure 4. The summary of the HOMO and LUMO energy levels estimated from the results of CV data. The details are described in the ESI.

Theoretical calculations

To obtain further insight into optical properties of the hypervalent Ge compounds, quantum chemical calculations with density functional theory (DFT) and time-dependent (TD)-DFT were performed (Figures 5 and S7–S17, Tables S5–S16). As a result, the effect of electronic perturbation induced by spiroconjugation on the azomethine- and azo-based π-conjugated systems was clearly revealed. The optimized structure of **GAmPh-Br** exhibits a partially distorted π-conjugated structure compared to that of **GAzPh-Br** because of steric hindrance from the methine proton (Figure 5). In contrast, both **GAmFl-Br** and **GAzFl-Br** exhibit highly planar π-conjugated systems as a result of steric effects from the *tert*-butyl groups on the germafluorene units, which is in good agreement with the results of the SC-XRD analyses. In contrast to the CV results, the HOMO energy levels are elevated and the LUMO energy levels are lowered in **GAmFl-Br** and **GAzFl-Br** compared to **GAmPh-Br** and **GAzPh-Br**, respectively (Figures 6 and S7). Therefore, the corresponding transition energies ($S_0 \rightarrow S_1$ for **GAmPh-Br** and **GAzPh-Br**, $S_0 \rightarrow S_1$ and S_2 for **GAmFl-Br** and **GAzFl-Br**) are reduced upon introduction of the

View Article Online
DOI: 10.1039/D6TC00672H

germafluorene units (Table S5). Based on the HOMO distribution, the significant increase in the HOMO energy level can be attributed to spiroconjugation in addition to σ–π conjugation between the azomethine- and azo-based π-conjugated systems and the germafluorene units (Figure 6). In addition, the reduction of the LUMO energy levels is likely attributable to effective π-conjugation originating from the planar π-conjugated system, rather than to spiroconjugation. This is because orbital interactions between the azomethine- and azo-based π-conjugated systems and the germafluorene units are hardly observed (Figures S9 and S11). The discrepancy between the CV and theoretical calculation results for the germafluorene-fused compounds may stem from the small energy difference between the HOMO and HOMO−1 (Figures S8–S11). Indeed, broadening at the onset of the oxidation curve was observed in the voltammogram of **GAmFl-Br** and **GAzFl-Br** (Figure S6). This should lead to underestimation of the HOMO energy levels.

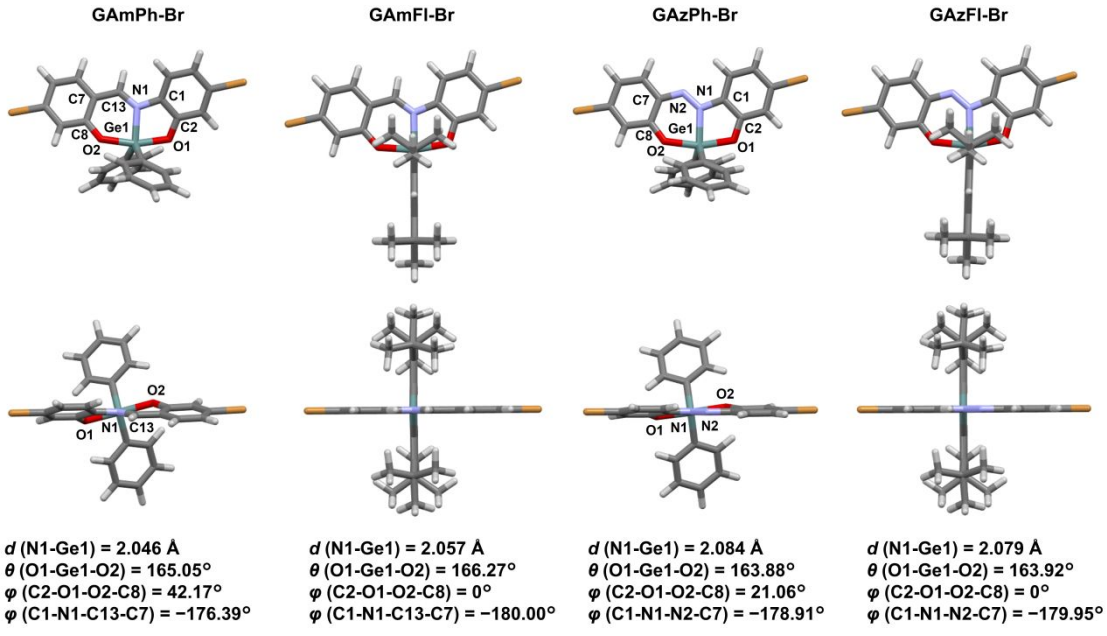

View Article Online
DOI: 10.1039/D6TC00672H

Figure 5. Optimized structures of hypervalent Ge monomers by quantum chemical calculations with DFT. Selected bond lengths (d), angles (θ), dihedral angles (φ) are shown.

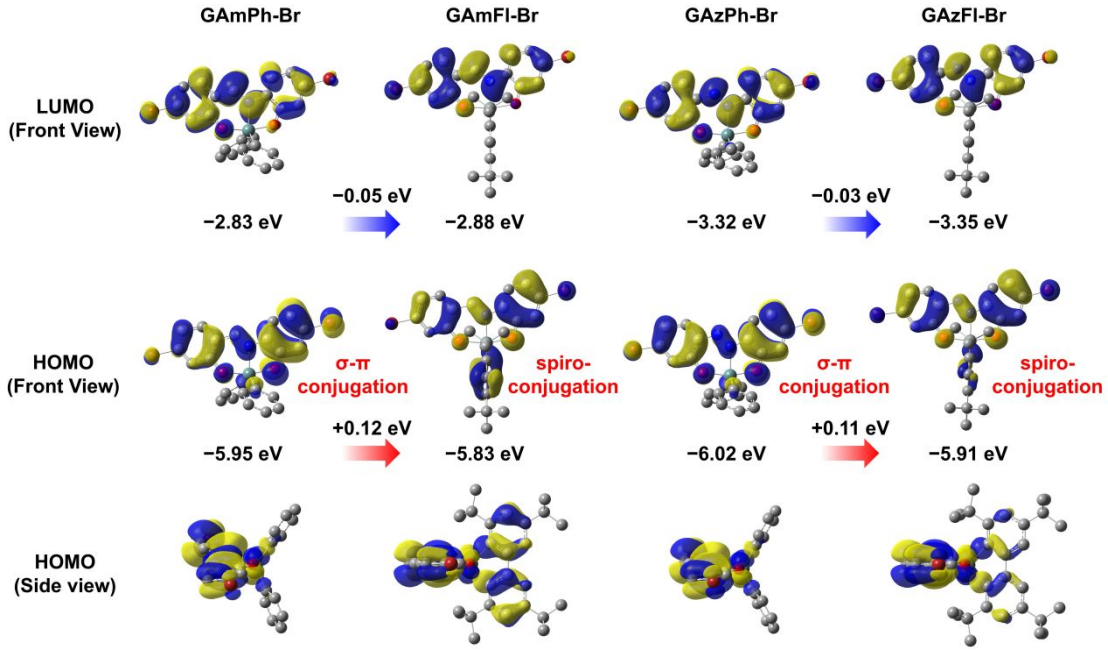

Figure 6. Kohn–Sham orbitals (isovalue = 0.02) with HOMO and LUMO energy levels of hypervalent Ge monomers. Hydrogen atoms are omitted for clarity.

Next, for theoretically estimating the electronic structures of polymers, the model compounds (**M-GAmFl-Ar** and **M-GAzFl-Ar** (Ar = **FL**, **BT**, and **CDT**)) were used for the reduction of the calculation cost. The results of **M-GAmFl-FL** are shown in Figure 7 as the representative example, and all results are described in the ESI (Figures S7, S12–S17 and Table S6). In the model compounds, the tendency of the changes in HOMO and LUMO energy levels is in good agreement with the experimental results from CV (Figure S7). This means that the constructed π-conjugated system can be categorized as a D–A π-

View Article Online
DOI: 10.1039/D6TC00672H

conjugated system. Interestingly, spiroconjugation was still observed in the HOMO of the π-conjugated system which extends over the hypervalent germafluorene-fused azomethine-based π-conjugated moiety as well as the electron-donating fluorene units (Figure 7). This effect likely contributes to an increase in the HOMO energy level and the consequent reduction of the energy gap of the π-conjugated polymer.

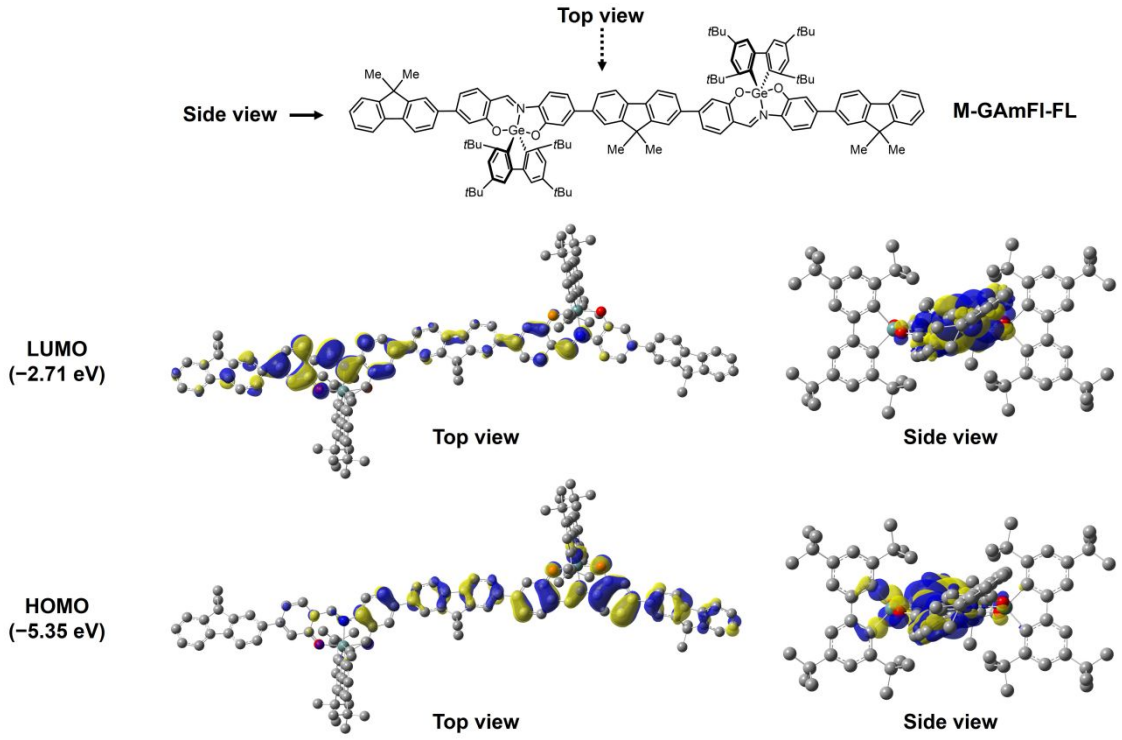

Figure 7. A chemical structure and Kohn–Sham orbitals (isovalue = 0.02) with HOMO and LUMO energy levels of **M-GAmFl-FL** as a model compound of **P-GAmFl-FL**.

Application for water-dispersible nanoparticles

NIR-light absorbing and emitting π-conjugated polymers are promising candidates for bioimaging applications owing to their high brightness, which originates from their large molar extinction coefficients as well as good emission efficiencies of π-conjugated

View Article Online
DOI: 10.1039/D6TC00672H

systems.[80] Therefore, to demonstrate the utility of our NIR light absorbing and emitting polymer for biological applications, we prepared a polymer NP dispersible in water.[41] The NP was fabricated using the micellizing agent Pluronic F-127, an amphiphilic molecule commonly employed for the biocompatible encapsulation of hydrophobic compounds.[81,82] We selected **P-GAzFl-CDT** as the NIR light absorbing and emitting polymer because it can exhibit the closest emission wavelength to the NIR-II region. The detailed procedure for the polymer NP preparation is shown in the ESI. As a result, the water-dispersible polymer NPs with an average size of 98.5 nm were obtained (Figure 8a). The polymer NPs showed maximum absorption and emission wavelengths in 807 and 1014 nm (Φ_{PL} < 0.1%), respectively (Figure 8b). The hypsochromic shift in the maximum absorption wavelength relative to those in solution and in the film state suggests the formation of H-aggregate-like structures.[83] It is known that the formation of H-aggregates reduces the transition probability of emissive states, leading to decreased luminescence intensity.[84] In addition, the presence of water in the surrounding environment likely affects the aggregates through polarity change, resulting in a bathochromic shift of the emission and a decrease in luminescence efficiency compared to the film state.[85] Thus, by creating hypervalent germanium compounds incorporating a germafluorene skeleton, we successfully developed NIR emissive materials that exhibit strong absorption and emission properties along with good processability. Although further studies, such as toxicity evaluation, cellular uptake behavior, and metabolic pathways of the prepared nanoparticles, are necessary for practical biological applications, we have successfully developed a novel polymer with advantageous optical properties.

View Article Online
DOI: 10.1039/D6TC00672H

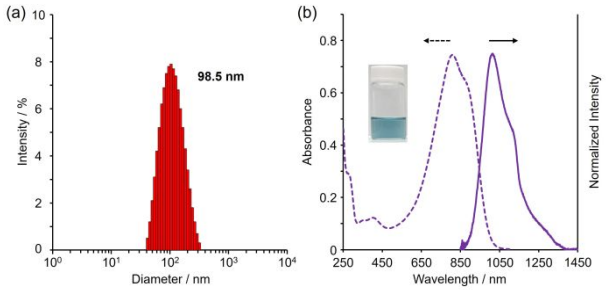

Figure 8. (a) UV−vis−NIR absorption (dotted line) and PL spectra (solid line), (b) a dynamic light scattering (DLS) profile of the polymer NP with **P-GAzFl-CDT** and Pluronic F-127 in deionized H_2O. The photograph of the polymer NP solution and the average particle size are denoted in each figure.

View Article Online
DOI: 10.1039/D6TC00672H

Conclusion

We synthesized novel five-coordinate hypervalent Ge compounds featuring germafluorene-fused azomethine and azo scaffolds. The monomers and polymers exhibited efficient light absorption and emission in the visible-to-NIR region (λ_{abs} = 505–902 nm, λ_{PL} = 667–1014 nm, Φ_{PL} up to 18.1%), owing to hypervalent Ge-centered spiroconjugation as well as the resulting planar and extended π-conjugated systems. In addition, efficient emission was also observed from polymer films because of suppression of interchain interactions with the bulky substituents on the germafluorene moiety. Furthermore, the high processability of the hypervalent Ge compounds enabled the fabrication of the water-dispersible NP exhibiting NIR-II emission. Our studies revealed the structural versatility of five-coordinate hypervalent Ge compounds incorporating germafluorene-fused azomethine and azo frameworks, and this versatility can be applied to the development of processable NIR light absorbing and emitting materials. These polymer materials can be used not only for bioimaging probes but also for enhanced security applications because of their optical invisibility in the NIR region to the human eye. Moreover, the hypervalent germafluorene-fused π-conjugated system is also expected to be applicable as a charge-transporting material by exploiting its narrow energy-gap properties. This can be achieved by reducing the steric substituents near the hypervalent germanium atom to enhance interchain π–π interactions.

View Article Online
DOI: 10.1039/D6TC00672H

Conflicts of interest

There are no conflicts to declare.

Acknowledgement

This work was partially supported by the National Research Foundation of Korea (NRF) grant funded by the Korea government (MSIT) (No. RS-2024-00406152), The Asahi Glass Foundation (for M.G.), Japan Society for the Promotion of Science (JSPS), a Grant-in-Aid for Scientific Research (B) (JP25K01818) (for M.G.) and (JP24K01570) (for K.T.).

Electronic Supplementary Information

Instrumentations, materials, synthetic procedures, characteristic data (^{1}H, $^{13}C\{^{1}H\}$ NMR spectra, and HRMS), experimental data (GPC profiles, single crystal X-ray structure analysis, PL decay curves, cyclic voltammograms, computational details for quantum chemical calculations, preparation methods of NPs, and coordinates for optimized structures with theoretical calculation)

View Article Online
DOI: 10.1039/D6TC00672H

References

1. A. Zampetti, A. Minotto and F. Cacialli, *Adv. Funct. Mater.*, 2019, **29**, 1807623.
2. M. Gon, S. Ito, K. Tanaka and Y. Chujo, *Bull. Chem. Soc. Jpn*, 2021, **94**, 2290–2301.
3. J. Wu, Z. Shi, L. Zhu, J. Li, X. Han, M. Xu, S. Hao, Y. Fan, T. Shao, H. Bai, B. Peng, W. Hu, X. Liu, C. Yao, L. Li, W. Huang, *Adv. Opt. Mater.*, 2022, **10**, 2102514.
4. J. Ye, D. Wang, H. Yao, H. Cong, Y. Shen and B. Yu, *Small*, 2025, **21**, 2409722.
5. S. A. Jenekhe and J. A. Osaheni, *Science*, 1994, **265**, 765–768.
6. A.-L. Thömmes and D. Scheschkewitz, *Angew. Chem. Int. Ed.*, 2026, **65**, e14344.
7. S. Ito, M. Gon and K. Tanaka, *Eur. J. Inorg. Chem.*, 2024, **27**, e202400180.
8. M. Gon, K. Tanaka, *Smart Mol.*, 2026, **4**, e20240064.
9. M. Gon, K. Tanaka and Y. Chujo, *Polym. J.*, 2018, **50**, 109–126.
10. J. B. Gilroy and E. Otten, *Chem. Soc. Rev.*, 2020, **49**, 85–113.
11. F. Vidal and F. Jäkle, *Angew. Chem. Int. Ed.*, 2019, **58**, 5846–5870.
12. Y. Adachi and J. Ohshita, "Germanium and Tin in Conjugated Organic Materials," In: *Main Group Strategies towards Functional Hybrid Materials* (eds. T. Baumgartner, F. Jäkle), 237–264, Wiley, Chichester, UK, 2018.
13. S. Yamaguchi, Y. Itami and K. Tamao, *Organometallics*, 1998, **17**, 4910–4916.
14. R. Inaba, K. Oka, T. Iwami, Y. Miyake, K. Tajima, H. Imoto and K. Naka, *Inorg. Chem.*, 2022, **61**, 7318–7326.
15. V. H. K. Fell, A. Mikosch, A.-K. Steppert, W. Ogieglo, E. Senol, D. Canneson, M. Bayer, F. Schoenebeck, A. Greilich and A. J. C. Kuehne, *Macromolecules*, **2017**, *50*, 2338–2343.

View Article Online
DOI: 10.1039/D6TC00672H

16. M. Planells, B. C. Schroeder and I. McCulloch, *Macromolecules*, **2014**, *47*, 5889–5894.
17. Y. Matsumura, K. Fukuda, S. Inagi and I. Tomita, *Macromol. Rapid Commun.*, **2015**, *36*, 660–664.
18. Y. Matsumura, M. Ishidoshiro, Y. Irie, H. Imoto, K. Naka, K. Tanaka, S. Inagi and I. Tomita, *Angew. Chem. Int. Ed.*, 2016, **55**, 15040–15043.
19. S. Morimoto, K. Tanimura, M. Gon, T. Suematsu, K. Okamoto, H. Watanabe, H. Taka, H. Kita and K. Tanaka, *Macromolecules*, 2024, **57**, 6531–6539.
20. K. Tanaka, Y. Chujo, *Chem. Lett.* **2021**, *50*, 269–279.
21. H. Watanabe, K. Tanaka and Y. Chujo, *Asian J. Org. Chem.*, 2022, **11**, e202200221.
22. E. Merino, *Chem. Soc. Rev.*, **2011**, *40*, 3835–3853.
23. C.-L. Liu, F.-C. Tsai, C.-C. Chang, K.-H. Hsieh, J.-L. Lin, W.-C. Chen, *Polymer*, **2005**, *46*, 4950–4957.
24. Y. Wang, J. Ma, Y. Jiang, *J. Phys. Chem. A*, **2005**, *109*, 7197–7206.
25. A. J. Blayney, I. F. Perepichka, F. Wudl, D. F. Perepichka, *Isr. J. Chem.* **2014**, *54*, 674–688.
26. N. C. Greenham, S. C. Moratti, D. D. C. Bradley, R. H. Friend, A. B. Holmes, *Nature* **1993**, *365*, 628–630.
27. A. Cembran, F. Bernardi, M. Garavelli, L. Gagliardi and G. Orlandi, *J. Am. Chem. Soc.*, 2004, **126**, 3234–3243.
28. T. Fujino, S. Y. Arzhantsev and T. Tahara, *J. Phys. Chem. A*, 2001, **105**, 8123–8129.
29. A. Izumi, R. Nomura and T. Masuda, *Macromolecules*, **2001**, 34, 4342–4347.
30. C.-P. Chang, C.-C. Wang, C.-Y. Chao and M.-S. Lin, *J. Polym. Res.*, 2005, **12**, 1–7.

View Article Online
DOI: 10.1039/D6TC00672H

31. A. V. Gaenko, A. Devarajan, L. Gagliardi, R. Lindh and G. Orlandi, *Theor. Chem. Acc.*, 2007, **118**, 271–279.

32. N. Kawatsuki, T. Washio, J. Kozuki, M. Kondo, T. Sasaki and H. Ono, *Polymer*, 2015, **56**, 318–326.

33. J. Yoshino, N. Kano and T. Kawashima, *Chem. Commun.*, 2007, 559–561.

34. J. Yoshino, N. Kano and T. Kawashima, *J. Org. Chem.*, 2009, **74**, 7496–7503.

35. M. Gon, K. Tanaka and Y. Chujo, *Chem. Rec.*, 2021, **21**, 1358–1373.

36. M. Nakamura, M. Gon and K. Tanaka, *Dalton Trans.*, 2025, **54**, 1079–1086.

37. H. Wang, Q. Li, P. Alam, H. Bai, V. Bhalla, M. R. Bryce, M. Cao, C. Chen, S. Chen, X. Chen, Y. Chen, Z. Chen, D. Dang, D. Ding, S. Ding, Y. Duo, M. Gao, W. He, X. He, X. Hong, Y. Hong, J.-J. Hu, R. Hu, X. Huang, T. D. James, X. Jiang, G.- Konishi, R. T. K. Kwok, J. W. Y. Lam, C. Li, H. Li, K. Li, N. Li, W.-J. Li, Y. Li, X.-J. Liang, Y. Liang, B. Liu, G. Liu, X. Liu, X. Lou, X.-Y. Lou, L. Luo, P. R. McGonigal, Z.-W. Mao, G. Niu, T. C. Owyong, A. Pucci, J. Qian, A. Qin, Z. Qiu, A. L. Rogach, B. Situ, K. Tanaka, Y. Tang, B. Wang, D. Wang, J. Wang, W. Wang, W.-X. Wang, W.-J. Wang, X. Wang, Y.-F. Wang, S. Wu, Y. Wu, Y. Xiong, R. Xu, C. Yan, S. Yan, H.-B. Yang, L.-L. Yang, M. Yang, Y.-W. Yang, J. Yoon, S.-Q. Zang, J. Zhang, P. Zhang, T. Zhang, X. Zhang, X. Zhang, N. Zhao, Z. Zhao, J. Zheng, L. Zheng, Z. Zheng, M.-Q. Zhu, W.-H. Zhu, H. Zou and B. Z. Tang, *ACS Nano*, 2023, **17**, 14347–14405.

38. J. Luo, Z. Xie, J. W. Y. Lam, L. Cheng, H. Chen, C. Qiu, H. S. Kwok, X. Zhan, Y. Liu, D. Zhu and B. Z. Tang, *Chem. Commun.*, 2001, 1740–1741.

39. Y. Dong, J. W. Y. Lam, A. Qin, Z. Li, J. Sun, H. H.-Y. Sung, I. D. Williams and B. Z. Tang, *Chem. Commun.*, 2007, 40–42.

View Article Online
DOI: 10.1039/D6TC00672H

40. M. Gon, K. Tanaka and Y. Chujo, *Polym. J.*, 2023, **55**, 723–734.

41. M. Nakamura, I. Kanetani, M. Gon and K. Tanaka, *Angew. Chem. Int. Ed.*, 2024, **63**, e202404178.

42. C. Hotta, M. Nakamura, M. Gon and K. Tanaka, *Adv. Optical Mater.*, 2025, **13**, e01251.

43. M. Gon, K. Tanaka and Y. Chujo, *Chem. Eur. J.*, 2021, **27**, 7561–7571.

44. M. Gon, Y. Morisaki, K. Tanimura, K. Tanaka, *Dalton Trans.* **2024**, *53*, 11858–11866.

45. M. Gon, K. Tanimura, K. Okazaki, T. Kato, D. Nakauchi, N. Kawaguchi, T. Yanagida and K. Tanaka, *Polym. J.*, 2025, **57**, 567–573.

46. M. Gon, M. Yaegashi, K. Tanaka and Y. Chujo, *Chem. Eur. J.*, 2023, **29**, e202203423.

47. M. Gon, M. Yaegashi and K. Tanaka, *Bull. Chem. Soc. Jpn.*, 2023, **96**, 778–784.

48. M. Gon, S. Dekura, T. Akutagawa and K. Tanaka, *Chem. Eur. J.*, 2025, **31**, e202500506.

49. I. Kanetani, M. Gon and K. Tanaka, *Macromolecules*, 2025, **58**, 8447–8457.

50. K. Tanimura, M. Gon and K. Tanaka, *Inorg. Chem.*, 2023, **62**, 4590–4597.

51. K. Tanimura, M. Gon, K. Tanaka and Y. Chujo, *Adv. Funct. Mater.*, 2025, **35**, 2418600.

52. J. I. Musher, *Angew. Chem. Int. Ed. Engl.*, 1969, **8**, 54–68.

53. K.-Y. Akiba and Y. Yamamoto, *Heteroatom Chem.*, 2007, **18**, 161–175.

54. G. C. Pimentel, *J. Chem. Phys.*, 1951, **19**, 446–448.

55. R. J. Hach and R. E. Rundle, *J. Am. Chem. Soc.*, 1951, **73**, 4321–4324.

View Article Online
DOI: 10.1039/D6TC00672H

56. P. A. Cahill, C. E. Dykstra and J. C. Martin, *J. Am. Chem. Soc.*, 1985, **107**, 6359–6362.

57. T. Atsumi, T. Abe, K.- Akiba and H. Nakai, *Bull. Chem. Soc. Jpn.*, 2010, **83**, 892–899.

58. B. A. Jackson, J. Harshman and E. Miliordos, *J. Chem. Educ.*, 2020, **97**, 3638–3646.

59. M. C. Durrant, *Chem. Sci.*, 2015, **6**, 6614–6623.

60. M. Gon and K. Tanaka, *Eur. J. Org. Chem.*, 2024, **27**, e202400738.

61. M. Gon and K. Tanaka, *Bull. Chem. Soc. Jpn.*, 2025, **98**, uoaf085.

62. A. A. Diamantis, J. M. Gulbis, M. Manikas and E. R. T. Tiekink, *Phosphorus Sulfur Silicon Relat. Elem.* 1999, **150**, 251–259.

63. D. Basu, B. Ghosh, D. Srivastava, N. Patra and H. P. Nayek, *Dalton Trans.* 2024, **53**, 5648–5657.

64. H. E. Simmons and T. Fukunaga, *J. Am. Chem. Soc.*, 1967, **89**, 5208–5215.

65. A. Ozcelik, D. Aranda, R. Pereira-Cameselle, M. Talavera, B. Covelo, F. Santoro, Á. Peña-Gallego and J. L. Alonso-Gómez, *ChemPlusChem*, 2022, **87**, e202100554.

66. S. Liu, D. Xia and M. Baumgarten, *ChemPlusChem*, 2021, **86**, 36–48.

67. S. Morisako, K. Noro and T. Sasamori, *Inorganics*, 2021, **9**, 75.

68. K.-H. Lee, J. Ohshita, D. Tanaka, Y. Tominaga and A. Kunai, *J. Organomet. Chem.*, 2012, **710**, 53–58.

69. E. F. Perozzi and J. C. Martin, *J. Am. Chem. Soc.*, 1979, **101**, 1591–1593.

70. L. J. van der Boon, L. van Gelderen, T. R. de Groot, M. Lutz, J. C. Slootweg, A. W. Ehlers and K. Lammertsma, *Inorg. Chem.*, 2018, **57**, 12697–12708.

71. M. Nakamoto and K.-Y. Akiba, *J. Am. Chem. Soc.*, 1999, **121**, 6958–6959.

View Article Online
DOI: 10.1039/D6TC00672H

72. H. Lenormand, V. Corcé, G. Sorin, C. Chhun, L.-M. Chamoreau, L. Krim, E.-L. Zins, J.-P. Goddard and L. Fensterbank, *J. Org. Chem.*, 2015, **80**, 3280–3288.

73. S. Iwabuchi, T. Morofuji and N. Kano, *Dalton Trans.*, 2024, **53**, 10829–10833.

74. M. Saito, S. Imaizumi, T. Tajima, K. Ishimura and S. Nagase, *J. Am. Chem. Soc.*, 2007, **129**, 10974–10975.

75. A. S. Gowda, T. S. Lee, M. C. Rosko, J. L. Petersen, F. N. Castellano and C. Milsmann, *Inorg. Chem.*, 2022, **61**, 7338–7348.

76. M. Kosugi, K. Sasazawa, Y. Shimizu and T. Migita, *Chem. Lett.* 1977, **6**, 301–302.

77. D. Milstein and J. K. Stille, *J. Am. Chem. Soc.* 1978, **100**, 3636–3638.

78. C. M. Cardona, W. Li, A. E. Kaifer, D. Stockdale and G. C. Bazan, *Adv. Mater.*, 2011, **23**, 2367–2371.

79. J. Pommerehne, H. Vestweber, W. Guss, R. F. Mahrt, H. Bässler, M. Porsch and J. Daub, *Adv. Mater.*, 1995, **7**, 551–554.

80. K. Terayama, S. Habuchi and T. Michinobu, *J. Polym. Sci.*, 2023, **61**, 2276–2291.

81. X. Ye, J. Zhang, H. Chen, X. Wang and F. Huang, *ACS Appl. Mater. Interfaces*, 2014, **6**, 5113–5121.

82. C. S. A. Caires, R. C. Nascimento, L. O. Araujo, L. F. Aguilera, S. L. Oliveira and A. R. L. Caires, *ACS Omega*, 2025, **10**, 40111–40118.

83. M. M. O'Connor, S. C. Hayden, M. K. Gish, J. L. Ratkovec, L. H. Harmon, Y. Zhang, S. Barlow, S. R. Marder, O. G. Reid and G. Rumbles, *Sustain. Energy Fuels*, 2025, **9**, 3796–3807.

84. N. Hestand and F. C. Spano, *Chem. Rev.*, 2018, **118**, 7069–7163.

85. M. Homocianu, *Microchem. J.*, 2024, **198**, 110166.

View Article Online
DOI: 10.1039/D6TC00672H

All experimental and characterization data and detailed experimental procedures are available in the published article and ESI.